Open-Phase Fault Modeling and Optimized Fault-Tolerant Control of Dual Three-Phase Permanent Magnet Synchronous Machines

Guodong Feng, *Member, IEEE*, Chunyan Lai, *Member, IEEE*, Wenlong Li, *Senior Member, IEEE*, Jimi Tjong, and Narayan C. Kar, *Senior Member, IEEE*

***Abstract*—This paper investigates open-phase fault modeling and fault-tolerant control (FTC) of dual three-phase permanent magnet synchronous machines (DT-PMSMs). A comprehensive fault model that considers both the permanent magnet torque and reluctance torque under the open-phase fault is proposed first. This model shows that under open-phase fault the average torque of DT-PMSM will decrease, while torque ripple will increase significantly. Then, a novel optimized FTC approach is developed based on the proposed model, in which genetic algorithm (GA) is applied to optimize the stator currents to maximize the average torque and minimize the torque ripple under open-phase fault. The proposed fault model and GA-based FTC are applicable to both surface-mounted and interior DT-PMSMs. However, existing approaches neglecting the reluctance torque are only applicable to surfaced-mounted DT-PMSMs. Moreover, the proposed approach is simple in implementation as it employs the original control structure and it is capable of smooth switching between the healthy operation and FTC without inducing noticeable torque pulses. The proposed approach is demonstrated with design examples, compared with existing one and validated with experiments on a laboratory interior DT-PMSM.**

***Index Terms*—Dual three-phase permanent magnet synchronous machine (DT-PMSM), fault modeling, fault-tolerant control (FTC), multi-phase machine, open-phase fault.**

I. Introduction

MULTI-PHASE permanent magnet synchronous machines (PMSMs) are better than conventional three-phase PMSMs in terms of efficiency, torque density, and fault-tolerant capability [1]–[5]. Therefore, multi-phase PMSMs are attracting attentions of researchers from both industry and academia. Dual three-phase PMSM (DT-PMSM) is a popular multi-phase PMSM structure consisting of two sets of three-phase windings with isolated neutral points and phase shift of

Manuscript received October 17, 2018; revised December 31, 2018; accepted February 6, 2019. Date of publication February 20, 2019; date of current version August 29, 2019. Recommended for publication by Associate Editor J. Hur. *(Corresponding author: Guodong Feng.)*

G. Feng, W. Li, J. Tjong, and N. C. Kar are with the Department of Electrical and Computer Engineering, University of Windsor, Windsor, ON N9B 3P4, Canada (e-mail:

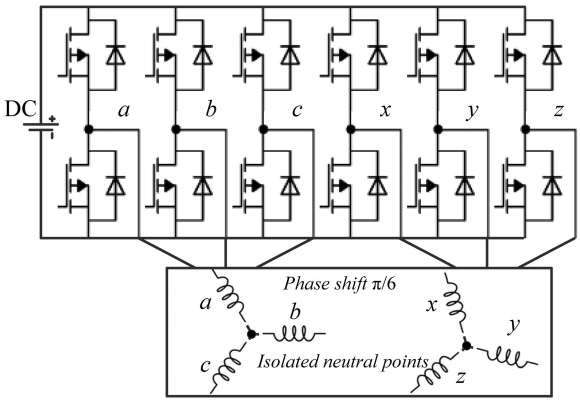

Fig. 1. Diagram of a DT-PMSM drive.

algorithm is employed to optimize the stator currents for FTC of a six-phase machine. However, aforementioned approaches focus on the surface-mounted PMSM, in which only the PM torque is considered. For the interior PMSM, the reluctance torque also contributes to a significant portion of the output torque [29]–[31]. The open-phase fault will also induce a decrease of the average torque and an increase of the torque ripple in the reluctance torque, which have not been considered in the existing approaches. Therefore, the existing approaches have limited applicability in interior DT-PMSMs.

This paper proposes a novel open-phase fault model for FTC of DT-PMSM by considering both PM torque and reluctance torque. Therefore, the proposed model is applicable to both the surface-mounted and interior DT-PMSMs. This model is then employed to analyze the DT-PMSM output torque, which will show that DT-PMSM will experience an average torque reduction and significant increase in the second and the fourth torque harmonics under open-phase fault. The proposed model suggests injecting the properly designed second harmonic components into the stator currents to cancel the induced torque ripple and improve the average torque. To this end, this paper proposes to employ genetic algorithm (GA) to optimize the stator currents to maximize the average output torque and minimize the torque ripple for FTC of DT-PMSMs. The proposed GA-based FTC also considers the overcurrent protection as a design constraint. The proposed approach is applicable to both the surfaced-mounted and interior DT-PMSMs. During the control, the optimized currents will be added to the original stator currents, which do not involve any control structure modification and thus is simple in implementation. Moreover, the proposed approach enables the smooth switching between healthy operation and FTC without inducing noticeable torque pulses, which has not been reported in existing approaches but is critical in practical applications to ensure the drive performance. The proposed approach is evaluated with both simulation and experimental tests on a laboratory interior DT-PMSM drive.

II. VSD-Based Healthy DT-PMSM Model

Fig. 1 presents the schematic diagram of a typical DT-PMSM drive. The DT-PMSM consists of two-sets of three-phase windings with isolated neutral points to eliminate the zero-sequence currents [39]. Without loss of generality, we use (*a*, *b*, *c*) and (*x*, *y*, *z*) to denote the two sets of windings, as shown in Fig. 1. The phase shift between *abc* and *xyz* windings is $\pi/6$, which is one of the most popular dual three-phase configurations. In fact, $\pi/6$ phase-shift can result in a larger torque density and a lower torque ripple, and under one set of three-phase opened the unbalanced magnetic force does not exist in this configuration [36]. This paper investigates modeling and control of DT-PMSM with one-phase opened. This section discusses the vector space decomposition (VSD) model of DT-PMSMs under the healthy condition.

The VSD model introduces a transformation matrix to convert the phase voltage, current, resistance, inductance, and flux linkage in the *abcxyz* frame into DQ_1, DQ_2, and O_1O_2 frames [32]–[35]. Since there are no currents in the O_1O_2 frame for the DT-PMSM under investigation, the O_1O_2 frame is independent from DT-PMSM modeling and control; thus, it is neglected [38]. Considering only DQ frames, the transformation matrix is given in the following equation:

$$\boldsymbol{T}_{\mathrm{DQ}}=\frac{1}{3}\begin{bmatrix}\cos\theta & -\cos\theta_1 & -\cos\theta_0 & -\sin\theta_1 & \sin\theta_0 & -\sin\theta\\ -\sin\theta & \sin\theta_1 & \sin\theta_0 & \cos\theta_1 & \cos\theta_0 & -\cos\theta\\ -\sin\theta & \sin\theta_1 & \sin\theta_0 & -\cos\theta_1 & -\cos\theta_0 & \cos\theta\\ -\cos\theta & \cos\theta_1 & \cos\theta_0 & \sin\theta_1 & \sin\theta_0 & -\sin\theta\end{bmatrix} \tag{1}$$

where $\theta_0=\theta-\pi/3$, $\theta_1=\theta+\pi/3$, θ is rotor electrical position, $\boldsymbol{T}_{\mathrm{DQ}}$ is the transformation matrix, and $\boldsymbol{T}_{\mathrm{DQ}}{}^{-1}$ is defined as $3\boldsymbol{T}_{\mathrm{DQ}}^{T}$.

In the *abcxyz* frame, the DT-PMSM model can be denoted as

$$\begin{cases}u_{abcxyz}=\mathbf{R}i_{abcxyz}+\dot{\lambda}_{abcxyz}\\ \lambda_{abcxyz}=\mathbf{L}i_{abcxyz}+\lambda_{PM,abcxyz}\end{cases} \tag{2}$$

where P_{abcxyz} with $P=u$, i, λ, or λ_{PM} denotes the vector of the phase voltage, current, flux linkage, or PM flux linkage in the *abcxyz* frame, respectively; the inductance matrix is $\boldsymbol{L}=[L_{ij}]$ with L_{ij} being the phase self-inductance for $i=j$ and the mutual inductance between phase i and phase j for $i\neq j$; $\boldsymbol{R}=\mathrm{diag}\,[R\ R\ R\ R\ R\ R]$ is the resistance matrix with R being the phase winding resistance.

In the VSD model, (1) is applied to (2) and two set of DQ frames, DQ_1 and DQ_2, are introduced. The VSD-based DT-PMSM voltage and torque equations can be denoted as

$$\begin{aligned}\mathrm{DQ}_1&:\begin{cases}u_{d1}=Ri_{d1}+L_{d1}\dot{i}_{d1}-\omega_e L_{q1}i_{q1}\\ u_{q1}=Ri_{q1}+L_{q1}\dot{i}_{q1}+\omega_e L_{d1}i_{d1}+\omega_e\Lambda_0\end{cases}\\ \mathrm{DQ}_2&:\begin{cases}u_{d2}=Ri_{d2}+L_{d2}\dot{i}_{d2}-\omega_e L_{q2}i_{q2}\\ u_{q2}=Ri_{q2}+L_{q2}\dot{i}_{q2}+\omega_e L_{d2}i_{d2}\end{cases}\end{aligned} \tag{3}$$

$$t_e=3P\left(\Lambda_0 i_{q1}+\left(L_{d1}-L_{q1}\right)i_{d1}i_{q1}\right) \tag{4}$$

where the variable with subscript "1" is in the DQ_1 frame and the variable with subscript "2" is in the DQ_2 frame; u_{d1}, u_{q1}, i_{d1}, i_{q1}, L_{d1}, and L_{q1} are the voltages, currents, and inductances in the DQ_1 frame, and similar for the ones with subscript "2"; ω_e is the rotor electrical speed, which is the same for DQ_1 and

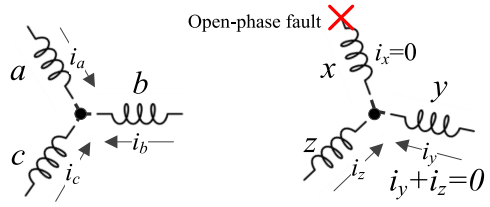

Fig. 2. DT-PMSM with phase x under open-phase fault.

DQ_2 frames; and Λ_0 is the PM flux linkage. t_e is the output torque and P is the number of pole pairs. Proof to (4) is given in Appendix A.

From the torque model (4), the currents i_{d2} and i_{q2} have no contribution to torque production and thus are controlled to be zero in VSD-based DT-PMSM control. However, the proposed fault model will show that under open-phase fault, the currents in both DQ_1 and DQ_2 frames will be controlled to be non-zero in order to ensure the drive performance. This paper focuses on modeling and optimized control of the DT-PMSM under open-phase fault to achieve the maximized average torque and minimized torque ripple.

III. Comprehensive DT-PMSM Open-Phase Fault Model

This section presents modeling of DT-PMSM under open-phase fault, in which both PM torque and reluctance torque will be considered. Compared with existing models, the proposed one is applicable to both the surface-mounted and the interior DT-PMSMs.

Let i_{dq} in (5) be the current vector in DQ_1 and DQ_2 frames under the healthy condition and let i_{abcxyz} in (6) be the six-phase current vector under the healthy condition:

$$i_{dq} = [i_{d1}\, i_{q1}\, i_{d2}\, i_{q2}]^T \tag{5}$$

$$i_{abcxyz} = [i_a\, i_b\, i_c\, i_x\, i_y\, i_z]^T. \tag{6}$$

In the VSD model, $i_{dq} = \boldsymbol{T}_{\mathrm{DQ}} i_{abcxyz}$, so i_{abcxyz} can be derived from i_{dq} as in the following equation, which is obtained by applying $\boldsymbol{T}_{\mathrm{DQ}}^{-1}$ to i_{dq}:

$$\begin{cases} i_a = i_{d1}\cos\theta - i_{d2}\sin\theta - i_{q1}\sin\theta - i_{q2}\cos\theta \\ i_b = i_{d1}\sin\theta_1 + i_{d2}\cos\theta_1 + i_{q1}\cos\theta_1 - i_{q2}\sin\theta_1 \\ i_c = -i_{d1}\sin\theta_2 - i_{d2}\cos\theta_2 - i_{q1}\cos\theta_2 + i_{q2}\sin\theta_2 \\ i_x = i_{d1}\cos\theta_1 + i_{d2}\sin\theta_1 - i_{q1}\sin\theta_1 + i_{q2}\cos\theta_1 \\ i_y = -i_{d1}\cos\theta_2 - i_{d2}\sin\theta_2 + i_{q1}\sin\theta_2 - i_{q2}\cos\theta_2 \\ i_z = -i_{d1}\sin\theta + i_{d2}\cos\theta - i_{q1}\cos\theta - i_{q2}\sin\theta \end{cases} \tag{7}$$

where $\theta_1 = \theta + \pi/3$ and $\theta_2 = \theta + \pi/6$. For healthy DT-PMSM control, i_{d2} and i_{q2} are controlled to be zero, while i_{d1} and i_{q1} are controlled based on the outer-loop torque or speed controller.

Without loss of generality, this paper assumes that phase x is under open-phase fault, which holds throughout this paper. As shown in Fig. 2, under fault, phase (x, y, z) currents should satisfy the following equation because phase (x, y, z) share the same neutral point:

$$i_x = 0,\ i_y = -i_z. \tag{8}$$

However, no constraint is imposed to phase (a, b, c) currents; thus, they are controlled to be the same as that in the healthy condition. Therefore, under open-phase fault, phase (a, b, c) currents are the same as (7), while phase (x, y, z) currents are in (8). Hence, based on (7) and (8), the six-phase current vector under open-phase fault, $i_{abcxyz,f}$, can be denoted as

$$i_{abcxyz,f} = [i_{a,f}\, i_{b,f}\, i_{c,f}\, i_{x,f}\, i_{y,f}\, i_{z,f}]^T \tag{9}$$

with

$$\begin{cases} i_{a,f} = i_a,\ i_{b,f} = i_b,\ i_{c,f} = i_c \\ i_{x,f} = 0,\ i_{y,f} = -i_{z,f} \end{cases} \tag{10}$$

where the subscript 'f' denotes that the parameter/variable is under the fault, which holds throughout this paper.

Applying (1) to (9) and (10), the actual current vector in DQ_1 and DQ_2 frames under open-phase fault, $i_{dq,f}$, can be derived as in (11) and (12) based on $i_{dq,f} = \mathbf{T}_{\mathrm{DQ}} i_{abcxyz,f}$

$$i_{dq,f} = [i_{d1,f}\, i_{q1,f}\, i_{d2,f}\, i_{q2,f}]^T \tag{11}$$

with

$$\begin{cases} i_{d1,f} = \frac{i_{d1}-i_{q2}}{2} - \frac{i_{y,f}}{\sqrt{3}}\cos\theta_1,\ i_{q1,f} = \frac{i_{d2}+i_{q1}}{2} + \frac{i_{y,f}}{\sqrt{3}}\cos\theta_3 \\ i_{d2,f} = \frac{i_{d2}+i_{q1}}{2} - \frac{i_{y,f}}{\sqrt{3}}\cos\theta_3,\ i_{q2,f} = \frac{i_{q2}-i_{d1}}{2} - \frac{i_{y,f}}{\sqrt{3}}\cos\theta_1 \end{cases} \tag{12}$$

where $\theta_1 = \theta + \pi/3$ and $\theta_3 = \theta - \pi/6$. Equations (5)–(12) can be summarized as Theorem 1.

Theorem 1: For the DT-PMSM with phase x opened, in order to guarantee the balance of the phase currents in phases y and z, the DQ_1 and DQ_2 frame currents $i_{dq,f}$ must satisfy (12).

Proof of Theorem 1: Applying $\boldsymbol{T}_{\mathrm{DQ}}{}^{-1}$ to $i_{dq,f}$ in (11), the phase currents under open-phase fault is $i_{abcxyz,f}$ in (9). It can be seen from (10) that $i_{x,f} = 0$ and $i_{y,f} + i_{z,f} = 0$; thus, the current balance condition is satisfied and Theorem 1 is proved.

From (12), under open-phase fault, the currents in DQ_1 and DQ_2 frames will contain low-order harmonics, which will result in harmonic components in the output torque. To obtain the torque model under open-phase fault, (11) and (12) are substituted into (4) and the torque model under open-phase fault is derived as in the following equation, where $L_\Delta = L_{d1} - L_{q1}$:

$$\begin{aligned} t_{e,f} &= 3P\left(\Lambda_0 i_{q1,f} + L_\Delta i_{d1,f} i_{q1,f}\right) \\ &= \frac{3P}{4}\begin{pmatrix} 2\left(i_{d2}+i_{q1}\right)\Lambda_0 + \left(i_{d2}+i_{q1}\right)\left(i_{d1}-i_{q2}\right)L_\Delta \\ +\frac{i_{y,f}}{3}\begin{pmatrix} 2\sqrt{3}\left(2\Lambda_0 + \left(i_{d1}-i_{q2}\right)L_\Delta\right)\cos\theta_3 \\ -2\sqrt{3}\left(i_{d2}+i_{q1}\right)L_\Delta\cos\theta_1 \\ -4L_\Delta i_{y,f}\cos\theta_1\cos\theta_3 \end{pmatrix} \end{pmatrix}. \end{aligned} \tag{13}$$

In DT-PMSM control, the phase current is generally controlled to be sinusoidal to avoid harmonic loss. Hence, during open-phase FTC, phase y current $i_{y,f}$ is controlled to satisfy

$$i_{y,f} = I_y\cos(\theta - \phi_y) \tag{14}$$

where I_y and ϕ_y are the magnitude and phase angle of $i_{y,f}$, respectively, and they will be optimized in the FTC.

In this way, the output torque of DT-PMSM under open-phase fault can be detailed as (15), which is obtained by substituting (14) into (13). It should be noted that the magnitude and phase angle of $i_{y,f}$ will be optimized for FTC

$$\begin{aligned}
t_{e,f} &= t_{e0} + t_{e2} + t_{e4} \\
t_{e0,1} &= 3P\left(\frac{(i_{d2}+i_{q1})}{2}\Lambda_0 + \frac{(i_{d2}+i_{q1})(i_{d1}-i_{q2})}{4}L_\Delta\right) \\
t_{e0,2} &= \frac{3P}{2}\left(CI_y\cos\left(-\phi_y+\frac{\pi}{6}\right) - DI_y\cos\left(-\phi_y-\frac{\pi}{3}\right)\right. \\
&\qquad \left. -\frac{L_\Delta I_y^2}{12}\cos\left(-2\phi_y-\frac{\pi}{6}\right)\right) \\
t_{e2} &= \frac{3PI_y}{2}\left(C\cos\left(2\theta-\phi_y-\frac{\pi}{6}\right) - D\cos\left(2\theta-\phi_y+\frac{\pi}{3}\right)\right. \\
&\qquad \left. -\frac{L_\Delta I_y}{6}\cos\left(2\theta+\frac{\pi}{6}\right)\right) \\
t_{e4} &= -\frac{PL_\Delta I_y^2}{8}\cos\left(4\theta-2\phi_y+\frac{\pi}{6}\right) \\
C &= \frac{2\Lambda_0+(i_{d1}-i_{q2})L_\Delta}{2\sqrt{3}}, D = \frac{(i_{d2}+i_{q1})L_\Delta}{2\sqrt{3}}
\end{aligned} \tag{15}$$

where $t_{e0,1}$ and $t_{e0,2}$ contain the dc component, t_{e2} contains second harmonic component, and t_{e4} contains fourth harmonic component.

Comparing the torque model (4) under the healthy condition with the torque model (15) under the fault condition, it can be observed that under open-phase fault

1) the average torque $(t_{e0,1}+t_{e0,2})$ has been reduced;
2) the second and fourth harmonic components (t_{e2} and t_{e4}) appear in the output torque;
3) the average torque $t_{e0,2}$ and the harmonic torques t_{e2} and t_{e4} are dependent on the control of the currents in DQ_1 and DQ_2 frames as well as the phase currents.

The proposed open-phase fault model in (9)–(15) is applicable to both the surface-mounted and interior DT-PMSMs. Based on the model, this paper will propose a novel GA- based optimized FTC for DT-PMSM to achieve the maximized average torque and minimized torque ripple.

IV. Optimized FTC of DT-PMSM With One-Phase Opened

A. Fault Tolerant Control—Problem Statement

The proposed FTC strategy is based on the following two observations from (15).

1) *Average torque improvement:* If i_{d1}, i_{q1} and $i_{y,f}$ are optimally designed, the average torque in $t_{e0,2}$ can also contribute to the average torque production.
2) *Torque ripple reduction:* If there are second harmonic components in i_{d1} and i_{q1}, there will be second and fourth harmonics in $t_{e0,1}$ and second harmonic in $t_{e0,2}$. With a proper design of the second harmonic components in i_{d1} and i_{q1}, it is possible to use the induced second and fourth harmonics in $t_{e0,1}$ and $t_{e0,2}$ to reduce or cancel the existing second and fourth harmonics t_{e2} and t_{e4}.

Above two observations can be summarized as follows: *if $i_{y,f}$ and the second harmonic components in i_{d1} and i_{q1} are optimized, the average torque in $t_{e,f}$ can be maximized while the torque ripple in $t_{e,f}$ can be minimized under open-phase fault.*

In this paper, the objective of FTC is to improve the average torque and reduce the torque harmonics. Assume that i_{d1}, i_{q1}, i_{d2}, i_{q2}, and $i_{y,f}$ are expressed as

$$\begin{cases} i_{d1} = I_{d1,0} + I_{d1,2}\cos(2\theta-\phi_d) \\ i_{q1} = I_{q1,0} + I_{q1,2}\cos(2\theta-\phi_q) \\ i_{d2} = i_{q2} = 0, \quad i_{y,f} = I_y\cos(\theta-\phi_y) \end{cases} \tag{16}$$

where $I_{d1,0}$ and $I_{q1,0}$ are the dc components for torque production and they can be obtained from existing MTPA control; $I_{d1,2}$, $I_{q1,2}$, ϕ_d, and ϕ_q are the magnitude and phase angle of the second current harmonics in i_{d1} and i_{q1}. The second current harmonics and $i_{y,f}$ are used to maximize the average torque and reduce the fault-induced torque ripple/harmonics.

Substituting (16) into (12), the DQ frame currents $i_{dq,f}$ under open-phase fault can be denoted as

$$\begin{cases} i_{d1,f} = \frac{I_{d1,0}+I_{d1,2}\cos(2\theta-\phi_d)}{2} - \frac{I_y\cos(\theta-\phi_y)}{\sqrt{3}}\cos\theta_1 \\ i_{q1,f} = \frac{I_{q1,0}+I_{q1,2}\cos(2\theta-\phi_q)}{2} + \frac{I_y\cos(\theta-\phi_y)}{\sqrt{3}}\cos\theta_3 \\ i_{d2,f} = \frac{I_{q1,0}+I_{q1,2}\cos(2\theta-\phi_q)}{2} - \frac{I_y\cos(\theta-\phi_y)}{\sqrt{3}}\cos\theta_3 \\ i_{q2,f} = -\frac{I_{d1,0}+I_{d1,2}\cos(2\theta-\phi_d)}{2} - \frac{I_y\cos(\theta-\phi_y)}{\sqrt{3}}\cos\theta_1. \end{cases} \tag{17}$$

Problem statement: The design task of FTC is to optimize DQ frame currents in (17) to maximize the dc component of $t_{e,f}$ in (15) and minimize the harmonic components of $t_{e,f}$. More specifically, given $I_{d1,0}$ and $I_{q1,0}$ from existing MTPA control, the objective of FTC is to find the optimal magnitudes ($I_{d1,2}$, $I_{q1,2}$, I_y) as well as the phase angles (ϕ_d, ϕ_q, ϕ_y) to maximize the average torque denoted by $\text{mean}(t_{e,f})$ and minimize the peak-to-peak torque ripple denoted by $\{\max(t_{e,f}) - \min(t_{e,f})\}$.

The FTC results in a multi-objective optimization problem and GA are employed for optimal FTC.

B. GA-Based FTC Design

In (17), the design parameters for FTC can be denoted as

$$D = [I_{d1,2}, I_{q1,2}, I_y, \phi_d, \phi_q, \phi_y] \tag{18}$$

and the two design objectives can be represented as

$$\begin{cases} g_1 = \text{maximize} \quad \text{mean}(t_{e,f}) \\ g_2 = \text{minimize} \ (\max(t_{e,f}) - \min(t_{e,f})). \end{cases} \tag{19}$$

The searching spaces of the design parameters in (18) can be determined as follows. For the phase angles, they should be within [0, 2π], which can be denoted as

$$\phi_d, \phi_q, \phi_y \in [0, 2\pi]. \tag{20}$$

For the current magnitudes, the phase current should be no more than the peak phase current $I_{\max}$ for the overcurrent protection, so the search space for the phase current is

$$I_y \in [0, I_{\max}]. \tag{21}$$

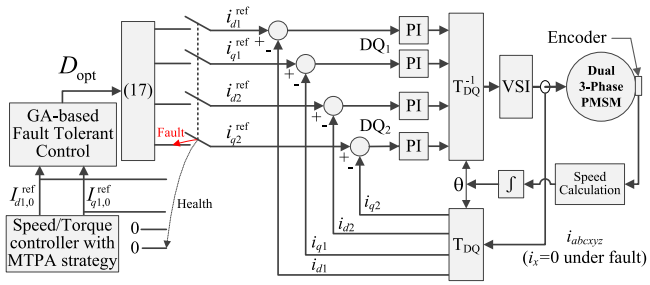

Fig. 3. DT-PMSM drive with the proposed FTC.

When the second harmonics currents are injected, the peak phase current should also be less than the maximum phase current, so substituting (17) into (7) and let the peak value be less than $I_{\max}$. In the proposed approach, the phase current under the open-phase fault is given in (10), so the search space can be calculated from

$$\max(I_{k,f}) < I_{\max},\ k = a, b, c. \tag{22}$$

GA is employed to optimize the design parameters in (18) to maximize g_1 and minimize g_2. The fitness function used in GA to evaluate each design parameter is defined as

$$F = \alpha_1 g_1 + \frac{\alpha_2}{g_2} \tag{23}$$

where α_i is the weight of the objective function g_i controlling the importance of g_i, $i = 1$ and 2. In (23), F increases when g_1 increases and g_2 decreases. Thus, the optimal currents will be obtained when F is maximized by GA. GA-based optimized FTC is summarized as follows.

Step 1. Initialization: Randomly generate a set of solutions according to (18) and (20)–(22), compute the fitness value F of each solution using (17), (14), (19), and (23), and save the best solution;

Set counter $n = 1$;

Step 2. Selection, crossover, and mutation: Perform selection, crossover, and mutation to current solutions to generate new solutions;

Step 3. Evaluation: Compute fitness value F of every new solution using (17), (14), (19), and (23) and save the best solution; $n = n + 1$; if n is less than the maximum iteration, go to Step 2.

Step 4: Output the best solution with maximum fitness value.

Remark 1: The proposed approach adds the optimized currents to existing stator currents for FTC, which does not involve any modification to the control structure and thus it is simple in implementation. Moreover, it is able to guarantee that the switching between the healthy operation and FTC is smooth.

C. Implementation of the Proposed FTC

The implementation of the proposed FTC in an existing DT-PMSM drive is shown in Fig. 3. In the proposed FTC, the inputs are DQ_1 frame reference currents from the outer speed/torque controller with the MTPA control strategy ($i_{d2} = i_{q2} = 0$), and the outputs are the DQ_1 and DQ_2 frame reference currents under open-phase fault. The PI current controllers will control the actual DQ_1 and DQ_2 frame currents to follow their references to produce the smooth output torque under open-phase fault. Here, the bandwidth of the PI current controllers should be set to be larger as the DQ_1 and DQ_2 frame currents under fault contain second harmonic components. It can be seen from Fig. 3 that the proposed FTC will add the optimized currents to the reference currents, which uses the same control structure and thus is simple in implementation.

TABLE I
FEA PARAMETERS OF THE TEST DT-PMSM

Rated current	15 A	NO. of poles/slots	8/48
Rated torque	75 Nm	L_Δ@ I_s=15 A,γ=30°	-21 mH
Rated speed	575 rpm	Magnet flux Λ_0	0.339 Wb
Rated voltage	140 V	Resistance	0.5 Ω

D. GA-Based FTC—Design Example

A laboratory DT-PMSM is employed to demonstrate the proposed GA-based FTC. The design parameters of the test motor are listed in Table I. As can be seen from Table I, this motor is an interior PMSM with the q-axis inductance being larger than the d-axis inductance in the DQ_1 frame. The MTPA control of interior DT-PMSM adopts "$i_{d1} < 0$" control, while the surface-mounted one adopts "$i_{d1} = 0$" control. Therefore, two conditions, C1) $I_{q1,0} = 10$ A, $I_{d1,0} = 0$ and C2) $I_{q1,0} = 9.4$ A, $I_{d1,0} = -3.4$ A, are considered to demonstrate that the proposed control is applicable to both the surface-mounted and interior PMSMs. Under $i_{d1} = 0$ control, the proposed approach is compared with the existing method. In the simulation, phase x is assumed to be opened and the harmonics in the PM flux linkages and inductances are neglected.

The parameters of GA are selected as follows: the population is 200, the maximum generation is 200, the probabilities of crossover and mutation are 0.8 and 0.2, respectively, and the weights for the fitness function are $\alpha_1 = 50$ and $\alpha_2 = 1$. The search space for the phase angles satisfies (20). For C1, the search space for I_y is [0, 10] and that for $I_{d1,2}$ and $I_{q1,2}$ is [0, 5]. For C2, the search space for I_y and that for $I_{d1,2}$ and $I_{q1,2}$ are [0, 11] and [0, 6], respectively. The proposed GA-based design approach is applied to find the optimal currents for the FTC of the test motor.

The optimized phase currents for C1 and C2 are shown in Figs. 4(a) and 5(a), respectively. As can be seen that phase x current is zero and phase y and z currents have the same magnitudes. The output torque under the healthy and fault conditions and FTC has been compared in Figs. 4(b) and 5(b). In these two figures, the output torque under fault denotes the case of letting $i_z + i_y = 0$. The performance has been compared in Table II. For C1, the output torque is 40.7 N·m under the healthy condition and it decreases to 27.8 N·m under the fault condition with a significant peak-to-peak torque ripple of 24.2 N·m. However, when the proposed FTC is applied, the output torque is increased to 33.3 N·m with a negligible peak-to-peak torque ripple of 0.3 N·m. Thus, the average torque has been improved by 5.5 N·m and torque ripple has been significantly reduced. For C2, similar results can be found. The average torque is improved

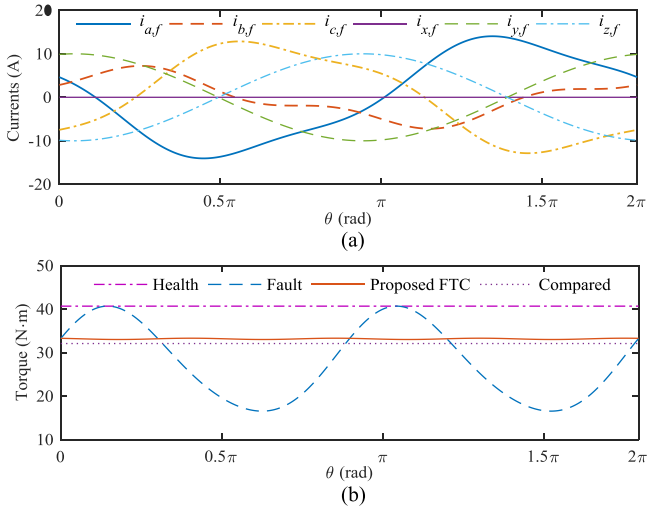

Fig. 4. Simulation results at C1. (a) Optimized phase currents. (b) Output torque under healthy and fault conditions and FTC.

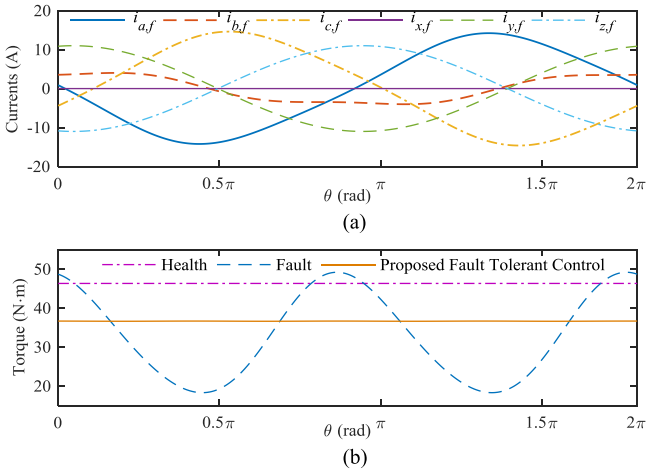

Fig. 5. Simulation results at C2. (a) Optimized phase currents. (b) Output torque under healthy and fault conditions and FTC.

TABLE II
PERFORMANCE COMPARISON UNDER HEALTHY AND FAULT CONDITIONS AND FTC

	Healthy (Nm)		Fault (Nm)		FTC (Nm)		
	DC	Ripple	DC	Ripple	Proposed		Compared in [9]
					DC	Ripple	DC
C1	40.7	/	27.8	24.2	33.3	0.3	32.08
C2	46.3	/	33.1	30.9	36.7	0.1	/

by 3.6 N·m and the torque ripple is significantly reduced under FTC. These results demonstrate that the proposed GA-based FTC can effectively improve the average torque of the test motor and reduce the torque ripple significantly for the DT-PMSM under open-phase fault.

The proposed approach is compared with the one in [9] that is developed for surface-mounted DT-PMSM. Under $i_{d1} = 0$ control in C1, the output torque of the compared method is compared in Fig. 4 and Table II. The compared method can achieve an average torque of 32 N·m, which, however, is 3.9% less than that in the proposed approach. Moreover, this method is not applicable to the interior DT-PMSM.

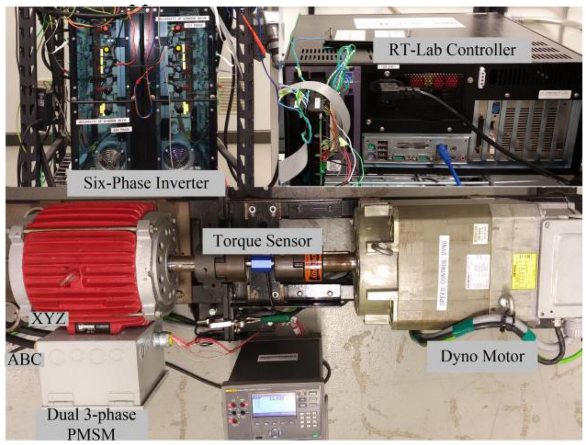

Fig. 6. Experimental setup for FTC of a DT-PMSM.

V. EXPERIMENTAL INVESTIGATIONS ON THE PROPOSED FTC

The proposed FTC is implemented in an FPGA-based Opal-RT controller and tested on a laboratory interior DT-PMSM with design parameters in Table I. As shown in Fig. 6, this test system is installed with a torque transducer, and the torque measurement will be used to evaluate the performance of the proposed FTC. During the experiment, the PWM signals of 12 power switches in the six-phase inverter are denoted by

$$\text{PWM} = [A_1\ A_2\ B_1\ B_2\ C_1\ C_2\ X_1\ X_2\ Y_1\ Y_2\ Z_1\ Z_2] \quad (24)$$

where $A_1, A_2, \ldots, Z_2$ can take values of either "1" or "0." To emulate open-phase fault in phase x, X_1, and X_2 in (24) are multiplied by zero and (24) is updated as

$$\text{PWM} = [A_1\ A_2\ B_1\ B_2\ C_1\ C_2\ 0\ 0\ Y_1\ Y_2\ Z_1\ Z_2]. \quad (25)$$

With (25), there will be no current flowing in phase x, which is equivalent to open-phase fault happened in phase x.

Five tests are conducted to evaluate the performance of the proposed FTC under various speed and load conditions. Specifically, Test 1 and Test 2 are conducted under "$i_{d1} = 0$" control and "$i_{d1} < 0$" control to demonstrate that the proposed approach is applicable to both surface-mounted and interior DT-PMSMs. In Test 1, the proposed approach is also compared with the method in [9] to show that the proposed approach can achieve a better performance. Test 3 is conducted at higher speeds, Test 4 is performed under torque and speed transient conditions, and Test 5 is conducted to demonstrate smooth switching between the healthy and FTC.

In Test 1, the motor is under "$i_{d1} = 0$" control and the DQ_1 axis reference currents are set to $I_{d1,0} = 0$ and $I_{q1,0} = 10$ A. Under the healthy condition, the currents in DQ_1 and DQ_2 frame and the output torque are shown in Fig. 7(a) and (b), respectively. From Fig. 7(a), there are no second harmonic components in the currents. From Fig. 7(b), the average torque is 38.3 N·m and there are no second and fourth torque harmonics.

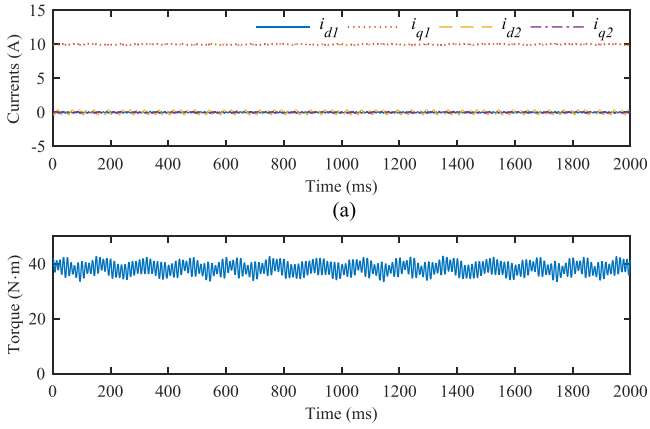

Fig. 7. Healthy condition in Test 1. (a) DQ_1 and DQ_2 currents. (b) Torque.

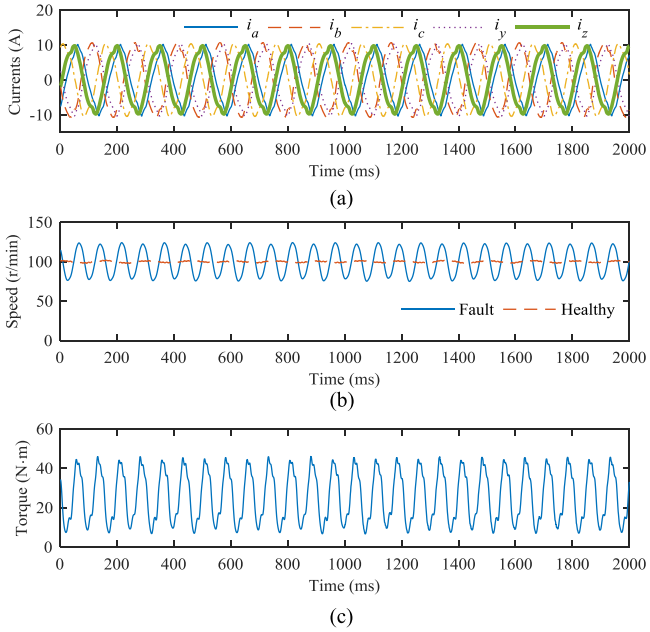

Fig. 8. Fault condition in Test 1. (a) Phase currents. (b) Speed. (c) Torque.

Under the fault condition, phase z current is set to be inverse of phase y current. The phase currents, speed, and output torque of the test motor are shown in Fig. 8(a), (b), and (c), respectively. From Fig. 8(c), the average torque is reduced to 25.7 N·m and there are significantly torque ripple in the output torque, in which the second harmonic magnitude is 14.3 N·m. Moreover, in Fig. 8(b), the motor speed consists of significant ripple with a peak to peak value of 46 r/min. Compared with healthy operation, the motor under fault is unable to deliver the smooth speed and torque without FTC.

Hence, the proposed FTC is applied to the test motor, and DQ_1 and DQ_2 currents, phase currents, speed, as well as the output torque are shown in Fig. 9(a)–(d), respectively. As can be seen from Fig. 9(a), during FTC the optimized second harmonics have been added into DQ frame currents to improve the average torque and reduce the torque ripple. The performance is compared in Table III. It can be seen that with the proposed

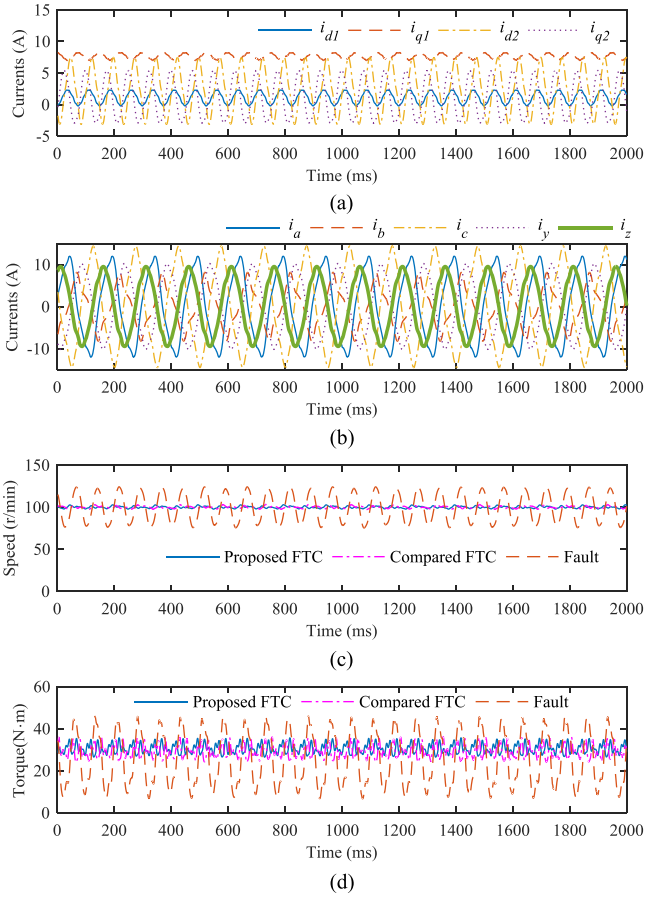

Fig. 9. Proposed FTC in Test 1. (a) DQ_1 and DQ_2 currents. (b) Phase currents. (c) Speed. (d) Torque.

TABLE III
PERFORMANCE COMPARISON IN TEST 1 AND TEST 2

		Average torque (Nm)	2nd torque harmonic (Nm)	Peak-to-peak speed ripple (r/min)
Test1	Healthy	38.3	/	2.7
	Fault	25.7	14.3	46
	FTC	30.5	0.8	2.8
	Method in [9]	29.36	1.1	4.3
Test2	Healthy	45.8	/	2.9
	Fault	18.9	16	64
	FTC	35.1	0.35	3.1

FTC, the test motor is able to deliver smooth speed and torque. Moreover, the average output torque is 30.5 N·m under the proposed FTC, which is improved by 4.8 N·m as compared to that under the fault condition. The second harmonic magnitude in the output torque is 0.8 N·m, which is greatly reduced as compared to 14.3 N·m under the fault condition. Moreover, the peak-to-peak speed ripple has been reduced from 46 to 2.8 r/min using the FTC.

In Test 1, the proposed approach is compared with the method in [9] under $i_{d1} = 0$ control. For the compared method, the speed and output torque of the test motor during FTC are shown in Fig. 9(c) and (d), respectively. The comparison with the proposed approach is listed in Table III. It can be seen that the

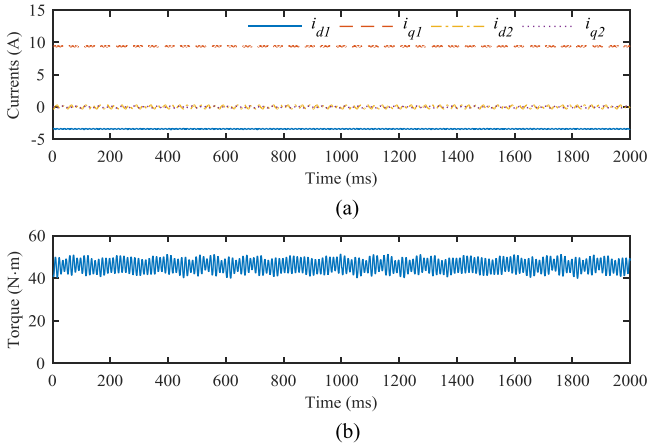

Fig. 10. Healthy condition in Test 2. (a) DQ_1 and DQ_2 currents. (b) Torque.

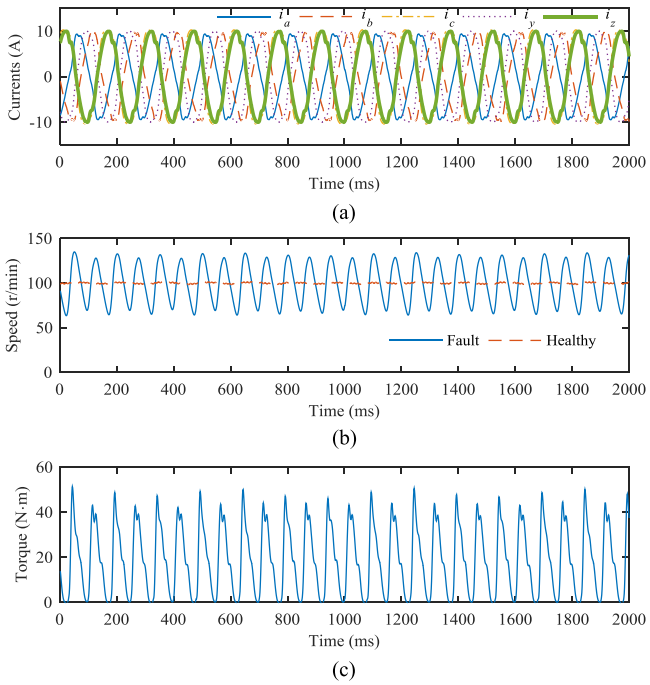

Fig. 11. Fault condition in Test 2. (a) Phase currents. (b) Speed. (c) Torque.

average torque in the compared method is 29.36 N·m, which is 3.74% less than that in the proposed approach, and the torque and speed ripples in the compared method are also larger than that in the proposed approach. Moreover, the compared method is not applicable to interior DT-PMSM.

In Test 2, the test motor is under "$i_{d1} < 0$" control with DQ_1 axis reference currents being set to $I_{d1,0} = -3.4$ A and $I_{q1,0} = 9.4$ A. Fig. 10 presents the DQ_1 and DQ_2 axis currents and output torque under the healthy condition. Fig. 11 shows the phase currents, speed, and output torque under the fault condition. Comparing Fig. 10 with Fig. 11, the output torque is 45.8 N·m under the healthy condition, and it is 18.9 N·m under the fault condition. Under the fault condition, the second torque harmonic magnitude is 16 N·m, which is about 85% of average torque, and the peak-to-peak speed ripple is 64 r/min, which is

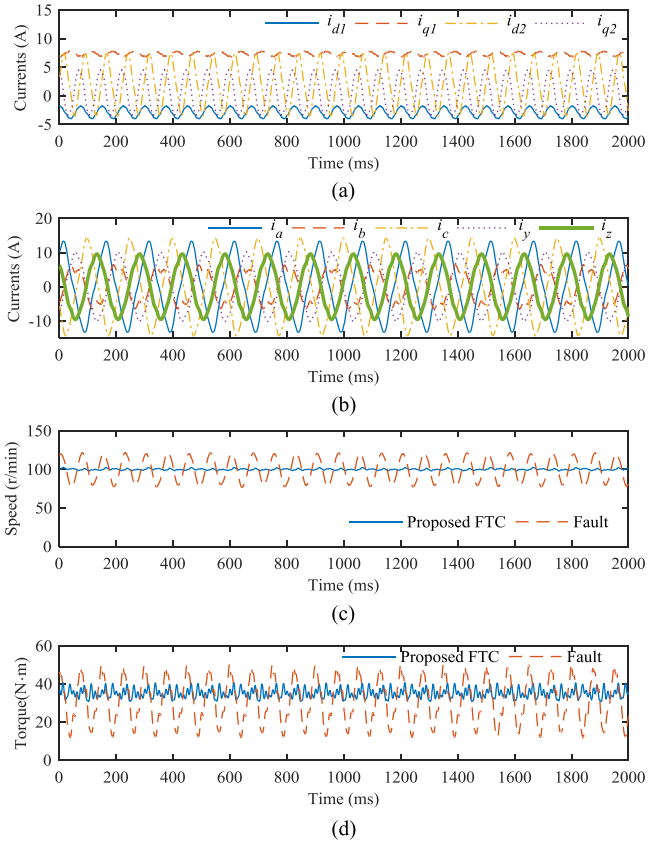

Fig. 12. Proposed FTC in Test 2. (a) DQ1 and DQ2 currents. (b) Phase currents. (c) Speed. (d) Torque.

64% of the average speed. So, the motor is unable to operate properly under the fault condition.

With the proposed FTC, the currents, motor speed, and the output torque are given in Fig. 12. It can be observed that the test motor is able to run properly. Performance comparison is listed in Table III. From Table III, the proposed FTC can improve the average torque to 35.1 N·m, that is, the average torque is improved by 85.7% as compared to that under the fault condition. Also, the induced second torque harmonic has been minimized to 0.35 N·m and speed ripple is reduced from 64 to 3.1 r/min. Hence, the proposed approach is capable of efficient FTC of DT-PMSM with improved average torque and reduced torque ripple.

In Test 3, the test motor operates at the speeds of 400 and 500 r/min, and the currents I_{d1} and I_{q1} are set to be -5 and 10 A, respectively. Fig. 13 presents the comparison of the motor speed and torque under healthy and fault conditions with the proposed FTC. The output torque is 53 N·m under the healthy condition. With the proposed FTC, the output torque is about 39 N·m and the peak-to-peak speed ripple is less than 2.5 r/min under open-phase fault. It can be seen that the test motor delivers less torque under the fault condition as compared to that under the healthy condition, which is due to the loss of one phase for torque production. However, compared with Figs. 8 and 11, the test motor with the proposed FTC can deliver smooth speed with improved average torque under open-phase fault at high speeds.

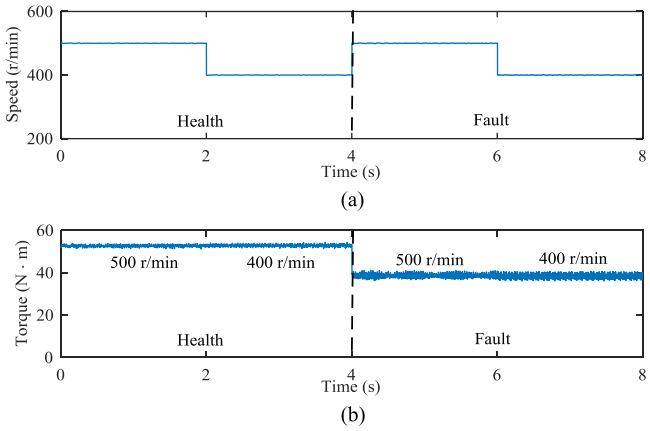

Fig. 13. Healthy and FTC comparison under high-speed conditions in Test 3. (a) Speed at 400 and 500 r/min. (b) Torque at 400 and 500 r/min.

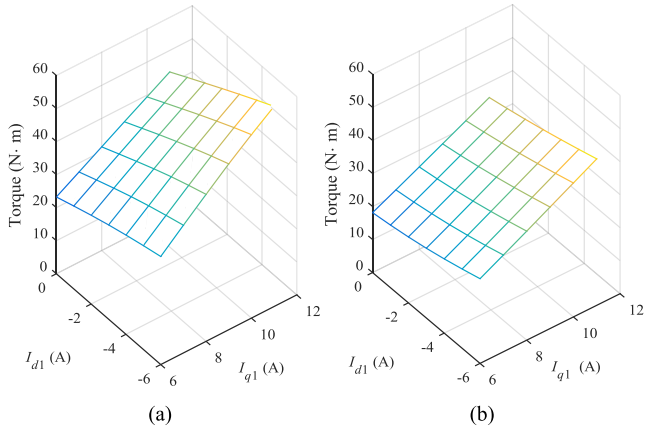

Fig. 14. Torque with respect to DQ_1 frame currents in Test 3. (a) Under the healthy condition. (b) Under open-phase fault with the proposed FTC.

Further tests are conducted to validate the proposed FTC under different loads at 400 r/min. Fig. 14 presents the comparison of the output torque with respect to DQ_1 frame currents under the healthy condition and open-phase fault with the proposed FTC. It should be noted that open-phase fault can result in significant torque and speed ripples, which could damage the mechanical structure of the test motor at high speeds. Therefore, tests under fault without FTC have not been conducted at high speeds. Indeed, Test 1 and Test 2 already show that the proposed FTC can improve the average torque and reduce the torque and speed ripples under open-phase fault. It can be seen from Fig. 15 that under open-phase fault, the torque delivered by the test motor increases as the current magnitude increases, but due to the loss of one phase, the test motor delivers less torque under fault as compared with that under the healthy condition. For instance, when I_{d1} and I_{q1} are -3 and 6 A, the output torque is 28.5 N·m under the healthy condition, and it is 21.1 N·m under open-phase fault with the proposed FTC.

For the operating conditions in Fig. 14, the motor efficiencies under the healthy condition and fault condition with the proposed FTC are compared in Fig. 15. From Fig. 15, the motor efficiency under the healthy condition is generally higher than that under the fault condition with the proposed FTC. This is

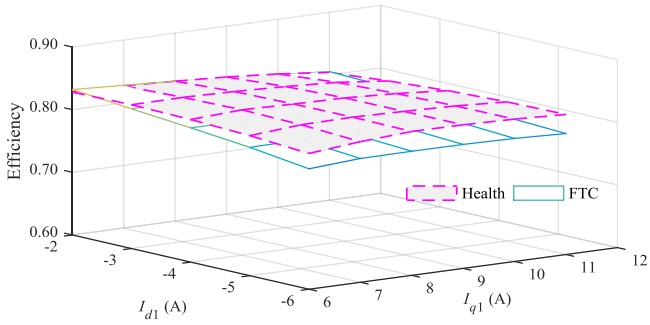

Fig. 15. Comparison of motor efficiency under the healthy condition and open-phase fault with the proposed FTC in Test 3.

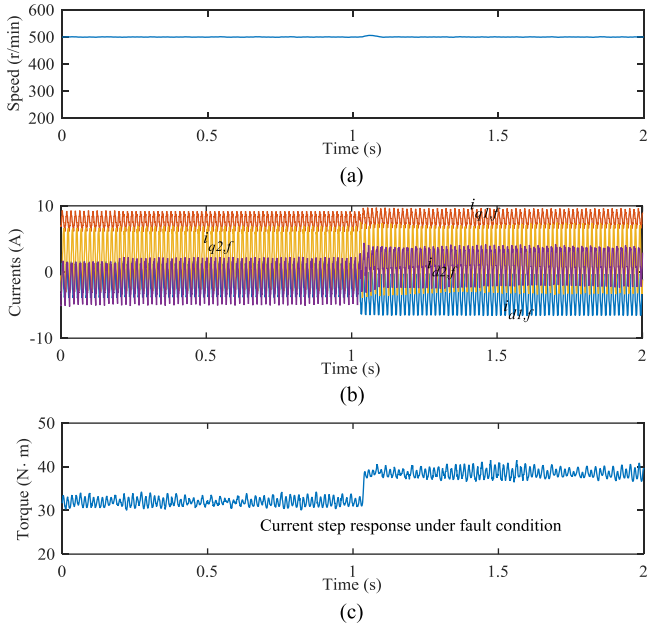

Fig. 16. FTC under the current transient condition in Test 4. (a) Speed. (b) Currents. (c) Torque.

because the motor delivers less torque with the same current magnitude under the fault condition. For instance, when I_{d1} and I_{q1} are -6 and 10 A, the motor efficiency under fault with the proposed FTC is 79.6% and it is 82.7% under the healthy condition.

Test 4 is conducted to validate the proposed FTC under the transient conditions. Fig. 16 presents the test motor speed, currents, and torque under current transient conditions with the proposed FTC, in which I_{d1} and I_{q1} change from 0 and 10 A to -5 and 10 A at $t = 1.1$ s and the motor speed is 500 r/min. It can be seen from Fig. 16 that the output torque increases from 31.9 to 38.9 N·m and the proposed FTC is capable of controlling the test motor under the current transient condition. Fig. 17 presents the test results under speed transient conditions. First, the test motor is under open-phase fault and the speed increases from 300 to 500 r/min with an increasing rate of 50 r/min, which is set by the speed dyno, and then, I_{d1} and I_{q1} are reduced from 8 and 0 A to -5 and 4 A at $t = 10$ s. It can be seen from Fig. 17 that with the proposed FTC, the test motor is able to operate stably under speed transient conditions without inducing any noticeable speed and torque ripples. Therefore, the proposed approach

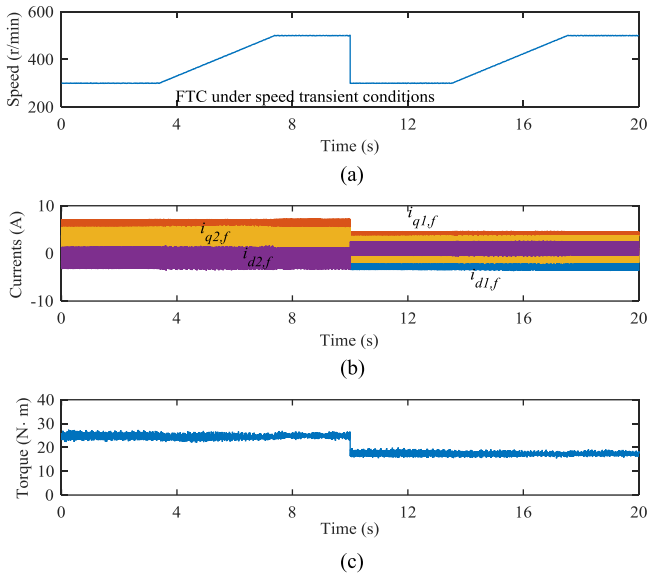

Fig. 17. FTC under the speed transient condition in Test 4. (a) Speed. (b) Currents. (c) Torque.

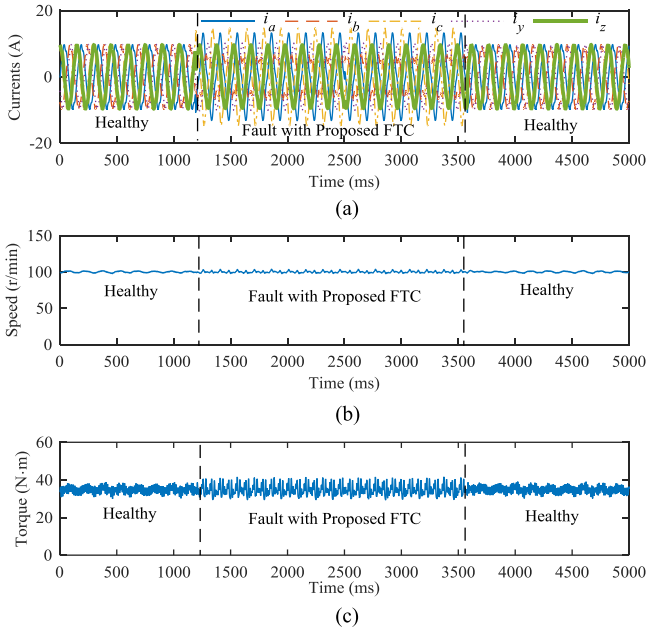

Fig. 18. Switching between the health and proposed FTC in Test 5. (a) Phase currents. (b) Output speed. (c) Output torque.

is capable of FTC under both current/torque and speed transient conditions.

In Test 5, the switching between the healthy operation and FTC is investigated. Fig. 18 presents the phase currents and output torque during the switching conditions. At 1.5 s, the test motor is under fault and the proposed FTC is applied. The motor is back to the healthy condition at about 3.5 s. From Fig. 18, the torque ripple under open-phase fault with the proposed FTC is slightly larger than that under the healthy condition, which is mainly due to two reasons. First, inaccurate parameters used for optimization will affect the control performance and result in a slight increase of torque ripple. On the other hand, DQ frame currents contain second harmonic during FTC and other current harmonic components induced by inverter distortion. According to [29], the current harmonics will also interact with the harmonics in the PM flux linkage to produce small torque ripple, which also contributes to a slight increase of torque ripple during FTC. This paper focuses on minimizing only the fault induced torque harmonics. However, it can be observed from Fig. 18 that there is not any noticeable ripple in the motor speed and torque during the switching between healthy control and proposed FTC. Therefore, the proposed FTC can be activated once the open-phase fault is detected, which ensures the drive performance and reliability as well as smooth switching between the healthy operation and FTC.

VI. Conclusion

This paper proposed a comprehensive motor model that is applicable to both the surface-mounted and interior DT-PMSMs under open-phase fault. An efficient GA-based FTC is developed for DT-PMSM with improved average torque and reduced torque and speed ripple. Extension of the proposed FTC to DT-PMSM with two-phase opened is discussed in Appendix B. The proposed FTC has a simple implementation and guarantees the smooth switching between the healthy operation and FTC, which is critical to ensure the drive performance and stability in the practical applications. The experimental results demonstrate that the proposed approach is effective for DT-PMSM FTC under various operating conditions and can achieve a better performance than the existing approach. Future work can be done in the following aspects. To consider the loss minimization in FTC, additional design objective of minimal motor loss should be included, and the fitness function will be revised accordingly. Optimal reference currents are independent from the motor speed, and a look-up table of optimized reference currents can be built at a specific speed condition. In this way, there will be no need to occupy the on-line computation resource to ensure efficient real-time FTC. Machine parameter variation will affect the optimal reference current generation, and thus incorporating online parameter estimation techniques can help further improve the control performance of the proposed approach.

Appendix A
Derivation of (4)

According to [29], t_e can be calculated from

$$t_e = P\left(\frac{1}{2} i_{abcxyz}^T \frac{d\boldsymbol{L}}{d\theta} i_{abcxyz} + i_{abcxyz}^T \frac{d\lambda_{PM,abcxyz}}{d\theta}\right) \quad (26)$$

where i_{abcxyz}, $\boldsymbol{L}$, and $\lambda_{\mathrm{PM},abcxyz}$ have the same definition as in (2).

Substituting $i_{dq} = \boldsymbol{T}_{dq} i_{abcxyz}$, $\boldsymbol{L}_{dq} = \boldsymbol{T}_{\mathrm{DQ}} \boldsymbol{L} T_{\mathrm{QD}}^{-1}$, and $\lambda_{\mathrm{PM},dq} = \boldsymbol{T}_{\mathrm{DQ}} \lambda_{\mathrm{PM},abcxyz}$ into (26), the result is

$$t_e = P\left(\begin{array}{l} \frac{1}{2}\left(\begin{array}{l} i_{dq}^T \left(\boldsymbol{T}_{\mathrm{DQ}}^{-1}\right)^T \frac{d\boldsymbol{T}_{\mathrm{DQ}}^{-1}}{d\theta} \boldsymbol{L}_{dq} i_{dq} \\ + i_{dq}^T \left(\boldsymbol{T}_{\mathrm{DQ}}^{-1}\right)^T \boldsymbol{T}_{\mathrm{DQ}}^{-1} \boldsymbol{L}_{dq} \frac{d\boldsymbol{T}_{DQ}}{d\theta} \boldsymbol{T}_{\mathrm{DQ}}^{-1} i_{dq} \end{array}\right) \\ + i_{dq}^T \left(\boldsymbol{T}_{\mathrm{DQ}}^{-1}\right)^T \frac{d\boldsymbol{T}_{DQ}^{-1}}{d\theta} \lambda_{PM,dq} \end{array}\right). \quad (27)$$

Substituting (1) into (27), the result is

$$t_e = 3P\left(\Lambda_0 i_{q1} + \left(L_{d1} - L_{q1}\right) i_{d1} i_{q1} + \left(L_{d2} - L_{q2}\right) i_{d2} i_{q2}\right). \tag{28}$$

Since $L_{d2} = L_{q2}$ [35], (28) can be rewritten as (4).

Appendix B
Discussions on DT-PMSM FTC With Two Phases Opened

This section discusses the extension of the proposed FTC to DT-PMSM with two phases under open-phase fault. Assume that the DT-PMSM has two phases opened, and let phases a and x be the faulty phases. In this case, the phase currents must satisfy the following equation in order to satisfy the current balance condition:

$$i_{a,f} = 0,\ i_{b,f} = -i_{c,f},\ i_{x,f} = 0,\ i_{y,f} = -i_{z,f}. \tag{29}$$

Applying (1) to $i_{abcxyz,f}$ in (29), the DQ frame currents under open-phase fault can be derived as

$$\begin{cases} i_{d1,f} = \frac{1}{2} i_{y,f} \sin\theta - \frac{\sqrt{3}}{6} i_{y,f} \cos\theta + \frac{\sqrt{3}}{3} i_{b,f} \sin\theta \\ i_{q1,f} = \frac{1}{2} i_{y,f} \cos\theta + \frac{\sqrt{3}}{3} i_{b,f} \cos\theta + \frac{\sqrt{3}}{6} i_{y,f} \sin\theta \\ i_{d2,f} = \frac{\sqrt{3}}{3} i_{b,f} \cos\theta - \frac{1}{2} i_{y,f} \cos\theta - \frac{\sqrt{3}}{6} i_{y,f} \sin\theta \\ i_{q2,f} = \frac{1}{2} i_{y,f} \sin\theta - \frac{\sqrt{3}}{6} i_{y,f} \cos\theta - \frac{\sqrt{3}}{3} i_{b,f} \sin\theta. \end{cases} \tag{30}$$

Therefore, for DT-PMSM with phases a and x opened, DQ_1 and DQ_2 frame currents must satisfy (30). Substituting (30) into (4), the torque model can be obtained, based on which the average torque and torque harmonics are available. Then, optimization algorithms such as GA can be applied to optimize the currents in (30) to achieve design objectives. In this way, the proposed FTC can be extended to the DT-PMSM with two phases opened. However, it should be noted that for the multiphase machine with more phases opened, a higher decoupling degree will inevitably affect the design of FTC and the control performance, and thus further research efforts are required.

References

[1] E. Levi, "Multiphase electric machines for variable-speed applications," *IEEE Trans. Ind. Electron.*, vol. 55, no. 5, pp. 1893–1909, May 2008.

[2] M. J. Duran and F. Barrero, "Recent advances in the design, modeling, and control of multiphase machines—Part II," *IEEE Trans. Ind. Electron.*, vol. 63, no. 1, pp. 459–468, Jan. 2016.

[3] C. Zhou, G. Yang, and J. Su, "PWM strategy with minimum harmonic distortion for dual three-phase permanent-magnet synchronous motor drives operating in the overmodulation region," *IEEE Trans. Power Electron.*, vol. 31, no. 2, pp. 1367–1380, Feb. 2016.

[4] A. K. M. Arafat and S. Choi, "Optimal phase advance under fault-tolerant control of a five-phase permanent magnet assisted synchronous reluctance motor," *IEEE Trans. Ind. Electron.*, vol. 65, no. 4, pp. 2915–2924, Apr. 2018.

[5] Y. Luo and C. Liu, "Elimination of harmonic currents using a reference voltage vector based-model predictive control for a six-phase PMSM motor," *IEEE Trans. Power Electron.*, to be published, doi: 10.1109/TPEL.2018.2874893.

[6] J. Karttunen, S. Kallio, P. Peltoniemi, and P. Silventoinen, "Current harmonic compensation in dual three-phase PMSMs using a disturbance observer," *IEEE Trans. Ind. Electron.*, vol. 63, no. 1, pp. 583–594, Jan. 2016.

[7] Y. Hu, Z. Q. Zhu, and M. Odavic, "Torque capability enhancement of dual three-phase PMSM drive with fifth and seventh current harmonics injection," *IEEE Trans. Ind. Appl.*, vol. 53, no. 5, pp. 4526–4535, Sep./Oct. 2017.

[8] J. Karttunen, S. Kallio, J. Honkanen, P. Peltoniemi, and P. Silventoinen, "Partial current harmonic compensation in dual three-phase PMSMs considering the limited available voltage," *IEEE Trans. Ind. Electron.*, vol. 64, no. 2, pp. 1038–1048, Feb. 2017.

[9] W. Wang, J. Zhang, M. Cheng, and S. Li, "Fault-tolerant control of dual three-phase permanent-magnet synchronous machine drives under open-phase faults," *IEEE Trans. Power Electron.*, vol. 32, no. 3, pp. 2052–2063, Mar. 2017.

[10] L. Cheng, Y. Sui, P. Zheng, P. Wang, and F. Wu, "Implementation of postfault decoupling vector control and mitigation of current ripple for five-phase fault-tolerant pm machine under single-phase open-circuit fault," *IEEE Trans. Power Electron.*, vol. 33, no. 10, pp. 8623–8636, Oct. 2018.

[11] X. Jiang, W. Huang, R. Cao, Z. Hao, and W. Jiang, "Electric drive system of dual-winding fault-tolerant permanent-magnet motor for aerospace applications," *IEEE Trans. Ind. Electron.*, vol. 62, no. 12, pp. 7322–7330, Dec. 2015.

[12] F. J. Lin, Y. C. Hung, J. C. Hwang, and M. T. Tsai, "Fault-tolerant control of a six-phase motor drive system using a Takagi–Sugeno–Kang type fuzzy neural network with asymmetric membership function," *IEEE Trans. Power Electron.*, vol. 28, no. 7, pp. 3557–3572, Jul. 2013.

[13] F. J. Lin, Y. C. Hung, and M. T. Tsai, "Fault-tolerant control for six-phase PMSM drive system via intelligent complementary sliding-mode control using TSKFNN-AMF," *IEEE Trans. Ind. Electron.*, vol. 60, no. 12, pp. 5747–5762, Dec. 2013.

[14] A. Mohammadpour and L. Parsa, "Global fault-tolerant control technique for multiphase permanent-magnet machines," *IEEE Trans. Ind. Appl.*, vol. 51, no. 1, pp. 178–186, Jan./Feb. 2015.

[15] B. A. Welchko, T. A. Lipo, T. M. Jahns, and S. E. Schulz, "Fault tolerant three-phase AC motor drive topologies: A comparison of features, cost, and limitations," *IEEE Trans. Power Electron.*, vol. 19, no. 4, pp. 1108–1116, Jul. 2004.

[16] B. Sen and J. Wang, "Stationary frame fault-tolerant current control of polyphase permanent-magnet machines under open-circuit and short-circuit faults," *IEEE Trans. Power Electron.*, vol. 31, no. 7, pp. 4684–4696, Jul. 2016.

[17] Y. Sui, P. Zheng, Z. Yin, M. Wang, and C. Wang, "Open-circuit fault-tolerant control of five-phase PM machine based on reconfiguring maximum round magnetomotive force," *IEEE Trans. Ind. Electron.*, vol. 66, no. 1, pp. 48–59, Jan. 2019. doi: 10.1109/TIE.2018.2829669.

[18] H. Zhou, W. Zhao, G. Liu, R. Cheng, and Y. Xie, "Remedial field-oriented control of five-phase fault-tolerant permanent-magnet motor by using reduced-order transformation matrices," *IEEE Trans. Ind. Electron.*, vol. 64, no. 1, pp. 169–178, Jan. 2017.

[19] A. Yepes, J. Doval-Gandoy, F. Baneira, and H. Toliyat, "Control strategy for dual three-phase machines with two open phases providing minimum loss in the full torque operation range," *IEEE Trans. Power Electron.*, vol. 33, no. 12, pp. 10044–10050, Dec. 2018.

[20] M. A. Shamsi-Nejad, B. Nahid-Mobarakeh, S. Pierfederici, and F. Meibody-Tabar, "Fault tolerant and minimum loss control of double-star synchronous machines under open phase conditions," *IEEE Trans. Ind. Electron.*, vol. 55, no. 5, pp. 1956–1965, May 2008.

[21] B. Tian, G. Mirzaeva, Q. T. An, L. Sun, and D. Semenov, "Fault-tolerant control of a five-phase permanent magnet synchronous motor for industry applications," *IEEE Trans. Ind. Appl.*, vol. 54, no. 4, pp. 3943–3952, Jul./Aug. 2018.

[22] S. Dwari and L. Parsa, "Fault-tolerant control of five-phase permanent-magnet motors with trapezoidal back EMF," *IEEE Trans. Ind. Electron.*, vol. 58, no. 2, pp. 476–485, Feb. 2011.

[23] M. Bermudez, I. Gonzalez-Prieto, F. Barrero, H. Guzman, M. J. Duran, and X. Kestelyn, "Open-phase fault-tolerant direct torque control technique for five-phase induction motor drives," *IEEE Trans. Ind. Electron.*, vol. 64, no. 2, pp. 902–911, Feb. 2017.

[24] I. González-Prieto, M. J. Duran, and F. J. Barrero, "Fault-tolerant control of six-phase induction motor drives with variable current injection," *IEEE Trans. Power Electron.*, vol. 32, no. 10, pp. 7894–7903, 2017.

[25] I. Arafat, S. Choi, and J. Baek, "Open-phase fault detection of a five-phase permanent magnet assisted synchronous reluctance motor based on symmetrical components theory," *IEEE Trans. Ind. Electron.*, vol. 64, no. 8, pp. 6465–6474, Aug. 2017.

[26] A. S. Abdel-Khalik, M. A. Elgenedy, S. Ahmed, and A. M. Massoud, "An improved fault-tolerant five-phase induction machine using a combined star/pentagon single layer stator winding connection," *IEEE Trans. Ind. Electron.*, vol. 63, no. 1, pp. 618–628, Jan. 2016.

[27] F. Mwasilu and J. W. Jung, "Enhanced fault-tolerant control of interior PMSMs based on an adaptive EKF for EV traction applications," *IEEE Trans. Power Electron.*, vol. 31, no. 8, pp. 5746–5758, Aug. 2016.
[28] Z. Liu, Z. Zheng, and Y. Li, "Enhancing fault-tolerant ability of a nine-phase induction motor drive system using fuzzy logic current controllers," *IEEE Trans. Energy Convers.*, vol. 32, no. 2, pp. 759–769, Jun. 2017.
[29] G. Feng, C. Lai, M. Kelly, and N. C. Kar, "Dual three-phase PMSM torque modelling and maximum torque per peak current control through optimized harmonic current injection," *IEEE Trans. Ind. Electron.*, vol. 66, no. 5, pp. 3356–3368, May 2019.
[30] N. Nakao and K. Akatsu, "Suppressing pulsating torques: Torque ripple control for synchronous motors," *IEEE Ind. Appl. Mag.*, vol. 20, no. 6, pp. 33–44, Nov. 2014.
[31] T. Sun and J. Wang, "Extension of virtual-signal-injection-based MTPA control for interior permanent-magnet synchronous machine drives into the field-weakening region," *IEEE Trans. Ind. Electron.*, vol. 62, no. 11, pp. 6809–6817, Nov. 2015.
[32] H. Eldeeb, A. S. Abdel-Khalik, and C. Hackl, "Dynamic modelling of dual three-phase IPMSM drives with different neutral configurations," *IEEE Trans. Ind. Electron.*, vol. 66, no. 1, pp. 141–151, Jan. 2019.
[33] J. Karttunen, S. Kallio, P. Peltoniemi, P. Silventoinen, and O. Pyrhönen, "Decoupled vector control scheme for dual three-phase permanent magnet synchronous machines," *IEEE Trans. Ind. Electron.*, vol. 61, no. 5, pp. 2185–2196, May 2014.
[34] S. Kallio, M. Andriollo, A. Tortella, and J. Karttunen, "Decoupled d-q model of double-star interior-permanent-magnet synchronous machines," *IEEE Trans. Ind. Electron.*, vol. 60, no. 6, pp. 2486–2494, Jun. 2013.
[35] Y. Hu, Z. Q. Zhu, and M. Odavic, "Comparison of two-individual current control and vector space decomposition control for dual three-phase PMSM," *IEEE Trans. Ind. Appl.*, vol. 53, no. 5, pp. 4483–4492, 2017.
[36] P. Xu *et al.*, "Analysis of dual three-phase permanent-magnet synchronous machines with different angle displacements," *IEEE Trans. Ind. Electron.*, vol. 65, no. 3, pp. 1941–1954, Mar. 2018.
[37] B. Lu and S. K. Sharma, "A literature review of IGBT fault diagnostic and protection methods for power inverters," *IEEE Trans. Ind. Appl.*, vol. 45, no. 5, pp. 1770–1777, Sep. 2009.
[38] Y. Hu, Z. Zhu, and K. Liu, "current control for dual three-phase permanent magnet synchronous motors accounting for current unbalance and harmonics," *IEEE J. Emerg. Sel. Topics Power Electron.*, vol. 2, no. 2, pp. 272–284, Jun. 2014.
[39] Y. Luo and C. Liu, "A simplified model predictive control for a dual three-phase PMSM with reduced harmonic currents," *IEEE Trans. Ind. Electron.*, vol. 65, no. 11, pp. 9079–9089, Nov. 2018.

Guodong Feng (M'15) received the B.S. and Ph.D. degrees in engineering from Sun Yat-sen University, Guangzhou, China, in 2010 and 2015, respectively.

From 2013 to 2015, he worked as a Research Assistant with Sun Yat-sen University and Carnegie Mellon University Shunde International Joint Research Institute, Shunde, China. He is currently a Postdoctoral Fellow with the Department of Electrical and Computer Engineering, University of Windsor, Windsor, ON, Canada. His research interests include advanced signal processing, optimization, and electrical machines and drives.

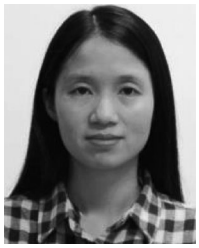

Chunyan Lai (M'17) received the B.S. degree in engineering from Sun Yat-sen University, China, in 2010, the Ph.D. degree in electrical and computer engineering from the University of Windsor, Windsor, ON, Canada, in 2017.

Between 2010 and 2013, she spent two and a half years in the industry in China. From 2017 to 2018, she was a Postdoctoral Fellow with University of Windsor. She is currently an Assistant Professor with the Department of Electrical and Computer Engineering, Concordia University, Montreal, QC, Canada. Her research areas include electric machine drives and controls and other power electronic related applications such as renewable energy.

Wenlong Li (SM'15) received the B.Eng. degree from Sichuan University, Chengdu, China, in 2005, the M.Eng. degree from the University of Science and Technology of China, Hefei, China, in 2008, and the Ph.D. degree from The University of Hong Kong, Hong Kong, China, in 2012, respectively.

He is currently a Professor with the School of Automation, Nanjing University of Science and Technology, Nanjing, China, and also a Visiting Scholar with the University of Windsor, Windsor, ON, Canada. He has authored or coauthored more than 70 peer-viewed technical papers and 3 invited book chapters. His research interests include electrical machine design, analysis, and applications.

Jimi Tjong received the B.Sc., M.Sc., and Ph.D. degrees in mechanical engineering from the University of Windsor, Windsor, ON, Canada, in 1980, 1984, and 1993, respectively.

He is currently an Adjunct Professor with the University of Windsor, the University of Toronto, Toronto, ON, and McMaster University, Hamilton, ON. His research interests include production and comprehensive design validation of components and systems for conventional and electrified vehicles and optimization of automotive test systems for cost, performance, and compatibility.

Narayan C. Kar (SM'07) received the B.S. degree in electrical engineering from the Bangladesh University of Engineering and Technology, Dhaka, Bangladesh, in 1992, and the M.S. and Ph.D. degrees in electrical engineering from the Kitami Institute of Technology, Hokkaido, Japan, in 1997 and 2000, respectively.

He is a Professor with the Department of Electrical and Computer Engineering, University of Windsor, Windsor, ON, Canada where he holds the Canada Research Chair Position in electrified transportation systems. His research interests include the analysis, design, and control of electrical machines for electrified vehicle applications.